Thermal analysis of AlGaN/GaN HEMTs considering anisotropic and inhomogeneous thermal conductivity

Yao Li[*, 1,2,3], Zixuan Zheng[2,3], Qun Li[2,3], Hongbin Pu[2,3]

[1] *Key Laboratory of Wide Band-gap Semiconductor Materials, Ministry of Education, Xidian University, CO 710071 China*

[2] *Department of Electronic Engineering, Xi'an University of Technology, Xi'an, CO 710048 China*

[3] *Xi'an Key Laboratory of Power Electronic Devices and High Efficiency Power Conversion, Xi'an, CO 710048 China*

Keywords GaN HEMT, Thermal conductivity, diamond, Temperature, Anisotropy

[*] Corresponding author: e-mail liyao@xaut.edu.cn

Abstract

To examine the differences of thermal characteristics introduced by material thermal conductivity, anisotropic polycrystalline diamond (PCD) and GaN are analyzed based on the accurate model of grain sizes in the directions of parallel and vertical to the interface and an approximate solution of the phonon Boltzmann transport equation. Due to the space-variant grain structures of PCD, the inhomogeneous-anisotropic local thermal conductivity, homogeneous-anisotropic thermal conductivity averaged over the whole layer and the typical values of inhomogeneous-isotropic thermal conductivity are compared with/without anisotropic GaN thermal conductivity. The results show that the considerations of inhomogeneous-anisotropic PCD thermal conductivity and anisotropic GaN thermal conductivity are necessary for the accurate prediction of temperature rise in the GaN HEMT devices, and when ignoring both, the maximum temperature rise is undervalued by over 16 K for thermal boundary resistance (TBR) of 6.5 to 60 m^2K/GW at power dissipation of 10

W/mm. Then the dependences of channel temperature on several parameters are discussed and the relations of thermal resistance with power dissipation are extracted at different base temperature. Compared with GaN, SiC and Si substrates, PCD is the most effective heat spreading layer though limited by the grain size at initial growth interface.

1. Introduction

Diamond composites is promising for thermal management of GaN high electron mobility transistors (HEMTs), due to its excellent heat spreading capability. Recent development of growth technology of polycrystalline diamond (PCD) facilitates the realization of large wafer sizes and a rather stable integration with GaN material. While the chemical vapor deposited PCD exhibits a columnar morphology with anisotropic grain size, which evolves with the distance from nucleation surface and is generally greater in the cross-plane direction than that in the in-plane direction. A. Sood et al[1] established a theoretical model of the PCD grain structures and related the anisotropy to phonon-grain boundary scattering, resulting in a rather practical expression of inhomogeneous-anisotropic PCD thermal conductivity. Based on the phonon Boltzmann transport equation, Jungwan Cho et al[2] modeled the in-plane thermal conductivity of GaN and calculated its relation with layer thickness. Therefore, for accurate prediction of thermal transport in GaN power devices, it's necessary to consider the inhomogeneity and anisotropy in both GaN and PCD thermal conductivity.

Several thermal studies on GaN-on-diamond devices taking anisotropic and inhomogeneous PCD thermal conductivity into account, J. Anaya et al[3] analyzed the effect of the PCD grain structure on the phonon scattering and on its thermal conductivity, establishing an accurate quantification of the thermal management in a GaN high power amplifier with PCD substrate. B. Zou

et al[4] extracted an effective thermal conductivity of the PCD substrate as "seen" by the device via finite element thermal simulation, considering the depth-dependent anisotropic thermal conductivity of PCD. By additionally counting the thickness dependence of in-plane thermal conductivity of GaN, Song et al[5] estimated the fundamental limits for near-junction conduction cooling of high power GaN-on-diamond devices. In light of these investigations, our study models the space-variant thermal conductivity of PCD substrate as well as anisotropic thermal conductivity of GaN, compares the junction temperature differences in GaN HEMT brought by different thermal conductivity models in GaN and PCD, and explores various impacting parameters, TBR, GaN layer thickness, gate pitch, heat source width, base temperature, dissipated power and substrate materials on device temperature rise. Our research may provide some instructions on the accurate thermal design of GaN HEMTs on PCD substrate.

2. Simulation details

To analyze the thermal characteristics of AlGaN/GaN HEMTs, the schematic cross-section of the device structure is shown in Figure 1 (a), which consists of a GaN buffer layer, an 20 nm-thick interfacial layer at GaN/diamond interface incorporating effective interfacial thermal resistance, a PCD substrate layer, an AuSn solder layer and a CuMo heat sink[4]. The simulated transistor is comprised of 12 gate fingers. Figures 1 (b) and (c) display the zoomed-in view and top view of GaN layer. The overall length and width of the chip are L and W, respectively. The heat sources modeled as cuboids with an embedding depth of D_e under GaN top surface is the representation of constant heat flux generated by dissipated power directly under the gate fingers, and gate/drain/source metallization is omitted due to the small structural complexity[4,6]. Here, a pitch spacing of S

between two adjacent heat sources is assumed. Due to the structural symmetry, only a quarter of the device is simulated, as illustrated in Figure 1(d). The structural parameters are summarized in Table 1[4,6].

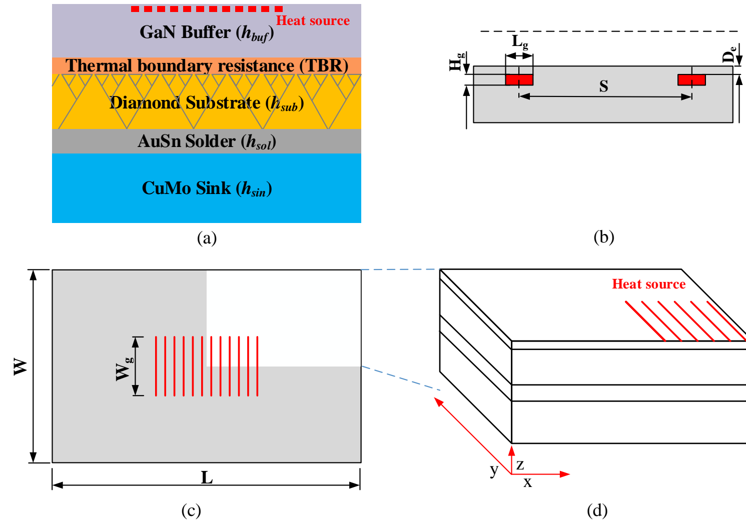

Figure 1 Schematic of cross section (a), zoomed-in view of heat sources (b), top view (c), and 3-D quarter simulation model of multi-fingers AlGaN/GaN HEMTs (d).

Table 1. Geometrical parameters of the simulated AlGaN/GaN HEMTs[4,6].

Parameter	Definition	Vaule
L	Device length	670 μm
W	Device width	530 μm
L_g	Heat source length	0.5 μm
W_g	Heat source width	240 μm
H_g	Heat source thickness	0.2 μm
S	Gate pitch	20 μm
h_{buf}	GaN thickness	1.4 μm
h_{sub}	Diamond thickness	100 μm

h_{sol}	AuSn thickness	20 μm
h_{sin}	CuMo thickness	4 mm
D_e	Embedding depth	0.2 μm
TBR	Thermal boundary resistance	6.5~60 m^2K/GW

For accurate estimation of the thermal characteristics, the anisotropic thermal conductivities of both GaN and diamond layers are calculated before simulation. According to the model from Ref. [2], the Umklapp and point defect scatterings are included to model the in-plane thermal conductivity of GaN, where only the strongest scatter, vacancy is considered as a type of point defect. As shown in Figure 2 (a), the curve with vacancy concentration n_v of 2.7×10^{18} cm^{-3} fits well with the in-plane thermal conductivity data[2,7], yielding $\kappa_{GaN,In\text{-}plane}$=130 W/(m·K) for layer thickness of 1.4 μm at room temperature. While for cross-plane thermal conductivity of GaN, a different heat flux suppression function that describes the reduction in phonon mean free paths due to boundary scattering is assumed based on the study by Zhang et al[8] and Sood et al [9]. Here, the parameter n_v is fitted as 4.5×10^{17} cm^{-3} with the reported data[10-14] and the resultant thermal conductivity at room temperature is ~160 W/(m·K), in accord with the result in Ref. [5]. For simplicity, the correlation between GaN thermal conductivity and temperature is taken as $k_{in\text{-}plane,\ cross\text{-}plane}(T/300)^{-1.4}$.

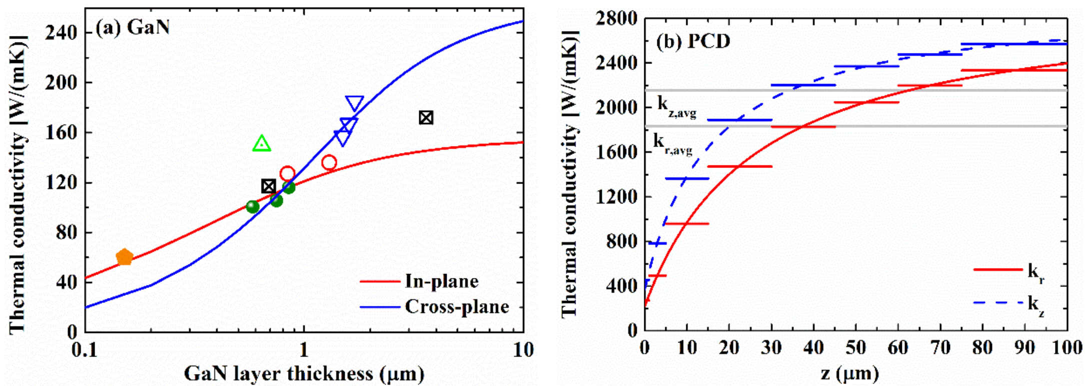

Figure 2 Variation of in-plane and cross-plane thermal conductivity of GaN and PCD layer with GaN layer thickness (a) and the distance z from the growth interface (b). The solid and open markers are in-plane and cross-plane thermal conductivity from literatures [2,7, 10-14].

As with PCD thermal conductivity, the key issue is to determine the average grain size at a certain distance from the growth interface based on phonon-grain boundary scattering. Following the model developed by A. Sood et al[1] that the columnar grains of PCD originating from the flat nucleation surface are trapezoidal regions, whose lateral sizes evolve linearly with the distance z from growth interface as $\langle d_r \rangle = \alpha z + d_0$ and the vertical size can be deduced as[1]

$$\frac{\langle d_z \rangle}{L_d} = \left(\xi + \frac{\beta}{\alpha} \right) \left[\frac{1}{\log(g)} \log \left(\frac{1+\frac{\beta}{\alpha}}{\xi + \frac{\beta}{\alpha}} \right) + 1 \right] - \frac{\beta}{\alpha} \tag{1}$$

where d_0 indicates the grain size at the nucleation interface, α is the grain evolution rate, L_d is the thickness of diamond film, $\xi = z/L_d$, $\beta = d_0/L_d$ and g represents the inverse of the grain survival rate.

Then the local thermal conductivities $\kappa_r(z)$ and $\kappa_z(z)$ are computed in light of phonon scattering in polycrystalline nanostructures proposed by Wang et al[15], where the local phonon mean free paths in the vertical λ_z and lateral directions λ_r can be calculated with local grain sizes $\langle d_z \rangle, \langle d_r \rangle$ and bulk phonon mean free path λ_{bulk} by Matthiessen's rule[1]

$$\lambda_{z,r}(z) = \left(1/\lambda_{bulk} + 1/0.75\langle d_{z,r} \rangle + 1/1.12\langle d_{r,z} \rangle \right)^{-1} \tag{2}$$

The local thermal conductivity $\kappa_{Int|z,r}(z)$ within each grain in two directions scales with $\lambda_{z,r}(z)/\lambda_{bulk}$, and equals $\kappa_{bulk}\lambda_{z,r}(z)/\lambda_{bulk}$, where λ_{bulk} is assumed to be 1 μm as the frequency independent bulk phonon mean free path (gray approximation) and thermal conductivity of bulk single crystal κ_{bulk} is taken as 3000 W/(m·K) based on the first-principle calculation of diamond by Li et al[1,16,17]. Finally, the net local conductivity can be obtained by considering the effect of grain

boundaries resistance R_{GB} and is given by

$$\kappa_{z,r}(z) = \left(1/\kappa_{Int|z,r}(z) + R_{GB}/\langle d_{z,r}\rangle\right)^{-1} \quad (3)$$

Figure 2(b) illustrates the resultant thermal conductivity of PCD as a function of the distance z from the growth interface with representative parameter values of g=2, α=0.066, d_0=130 nm and R_{GB}=0.1 m^2K/GW, according to simulations and calculations[1,4,17,18]. As shown, both κ_r(z) and κ_z(z) multiplies with increasing z due to the enlargement of PCD grain size. For simplicity, the spatial variations of κ_r and κ_z are discretized into 8 subsections (0-1, 1-5, 5-15, 15-30, 30-45, 45-60, 60-75, 75-100 μm) and the local average thermal conductivities of each sublayer are introduced to the simulation, as indicated by red and blue bars in Figure 2(b). For contrast, the thermal conductivities $\kappa_{r,avg}$ and $\kappa_{z,avg}$, averaged over the full thickness of PCD film in both directions are shown in gray lines.

To simulate the thermal characteristics of GaN HEMTs, a constant heat flux generated by dissipated power is applied directly under heat sources, and the power dissipation is set to 10 W/mm. The top AlGaN barrier layer is negligible in the analysis due to its minimal contribution on thermal resistance[4,6]. An isothermal surface of 300 K is applied at the bottom of the substrate and other external surfaces are assumed to convect naturally. Here, the natural air convection coefficient and ambient temperature are set as 20 W/(m^2K) [19,20] and 300 K. For accuracy, the temperature-dependent thermal conductivity of the substrate layer is considered. The thermal parameters of each layer used in the simulation are summarized in Table 2.

Table 2. Thermal parameters of each layer used in the simulation[21,22]

Material	Thermal conductivity [W/(m·K)]	Heat capacitance [J/(kg·K)]	Density (kg/m^3)	TBR (m^2K/GW)

Au (heat source)	317	129	19300	s
GaN	$k_{in\text{-}plane,\ cross\text{-}plane}(T/300)^{-1.4}$	490	6150	--
Diamond	$k_{r,z}(T/300)^{-0.55}$	520	3515	6.5[23]
Si	$150(T/300)^{-1.3}$	705	2329	3.4[24]
SiC	$420(T/300)^{-1.3}$	581	3100	5[13]
AuSn	57	128	14700	

3. Results and discussions

To assess the effect of PCD thermal conductivity on channel temperature of GaN-based HEMTs, we compare the cases with inhomogeneous and anisotropic thermal conductivity (red and blue bars in Figure 2(b)), homogeneous-anisotropic thermal conductivity ($\kappa_{r,avg}$ and $\kappa_{z,avg}$ mentioned above) and homogeneous-isotropic thermal conductivity (κ_r=κ_z=2000 W/(m·K)). The results are displayed in Figure 3 (a). As shown, inhomogeneous-anisotropic PCD thermal conductivity contributes most to the maximum channel temperature rise, while the impact of homogeneous-isotropic thermal conductivity is almost equal to that of homogeneous-anisotropic thermal conductivity with/without considering the anisotropy in GaN thermal conductivity. All types of PCD thermal conductivities help to raise the channel temperature with the increase of TBR, and the differences of maximum temperature rise originating from the inhomogeneous-anisotropic thermal conductivity with the others are relatively large at small TBR and decrease slightly for increasing TBR.

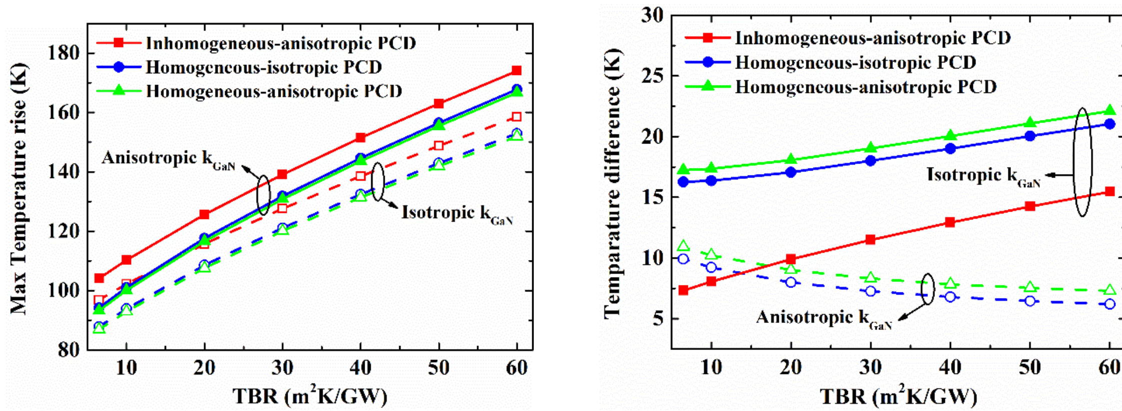

(a) (b)

Figure 3 Maximum temperature rise as a function of TBR for isotropic and anisotropic GaN thermal conductivity (a) and errors for neglecting neither the inhomogeneous-anisotropic PCD or anisotropic GaN versus TBR (b).

For quantitative interpretation of the impact of inhomogeneous-anisotropic PCD and GaN thermal conductivity, we calculate the temperature differences introduced by neglecting neither the inhomogeneous-anisotropic PCD or anisotropic GaN, whose values are obtained by subtracting from the results with inhomogeneous-anisotropic PCD and anisotropic GaN thermal conductivity. As Figure 3 (b) shows, the temperature difference of neglecting solely the anisotropy in GaN thermal conductivity increases from 7.3 to 15.5 K for TBR of 6.5~60 m^2K/GW, while the differences for ignoring the anisotropic/space-variant PCD thermal conductivity are relatively large at small TBR, about 10 K at TBR=6.5 m^2K/GW and reduce to 6~7 K for TBR of 60 m^2K/GW. For the case with homogeneous/isotropic PCD thermal conductivity and isotropic GaN thermal conductivity, the errors are the largest (over 15 K) at small TBR and display an increasing tendency when TBR increases. Since a high value of TBR impedes the effective thermal conduction from top GaN to bottom PCD substrate layer, the heat tends to be concentrated more on GaN layer and thus the accurate description of thermal conductivity in GaN than PCD matters with enlarging TBR. Accordingly, the resultant temperature differences with isotropic GaN thermal conductivity increase, while the errors originating from homogeneous/isotropic PCD thermal conductivity and anisotropic GaN thermal conductivity reduce with the increase of TBR.

Based on the above conclusion, the anisotropy of GaN thermal conductivity is included in the following discussion. Due to the thickness dependent in-plane thermal conductivity of GaN shown in

Figure 2 (a), the effect of GaN layer thickness on maximum temperature rise is analyzed in Figure 4. For thickness of 0.5~5 μm, the inhomogeneous-anisotropic PCD thermal conductivity contributes most to channel temperature, while homogeneous-isotropic and homogeneous-anisotropic PCD thermal conductivities affect almost equally. Similar to Refs. [21,25], an optimum GaN layer thickness exists due to the non-zero TBR and localized heating in active region of transistors, which is around 3 μm for TBR=10 m^2K/GW and is about 4 μm for TBR=30 m^2K/GW. In practice, for localized hotspot, the effect of GaN layer thickness on channel temperature is two-sided. On the one hand, the GaN layer needs to be thick enough to effectively conduct heat before through the highly resistive GaN/subtrate interface. On the other hand, a too thick GaN layer increases the thermal resistance due to the limited heat-spreading capability of GaN. Therefore, the optimum GaN layer thickness increases with the enlargement of TBR.

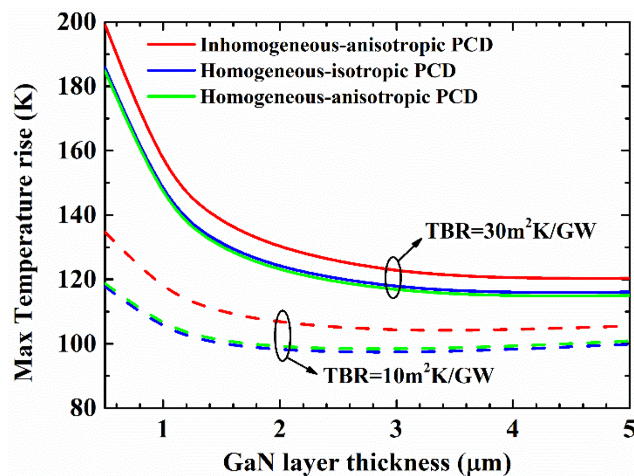

Figure 4 Maximum temperature rise versus GaN layer thickness for TBR of 10 and 30 m^2K/GW.

The interrelations between the anisotropy and inhomogeneity in PCD thermal conductivity and gate pitch/heat source width are evaluated in Figure 5 (a) and (b), respectively. As seen, for gate pitch of 2~50 μm, the maximum temperature rise resulting from homogeneous-isotropic PCD thermal conductivity is almost the same with that from homogeneous-anisotropic PCD thermal conductivity

and is lower than that from inhomogeneous-anisotropic PCD thermal conductivity. The maximum temperature rise is large for gate pitch of 2 μm and drastically reduces by ~60% for inhomogeneous-anisotropic PCD thermal conductivity and ~55% for homogeneous-isotropic/homogeneous-anisotropic PCD thermal conductivity with gate pitch increasing to 10 μm. As gate pitch enlarges further, the temperature slowly decreases. Therefore, restraining the length of gate pitch is an effective way to reduce the channel temperature. Figure 5 (b) displays that the impact of heat source width is limited, since the increment of maximum temperature rise is only 10 K~15 K as heat source width increases from 50 to 300 μm.

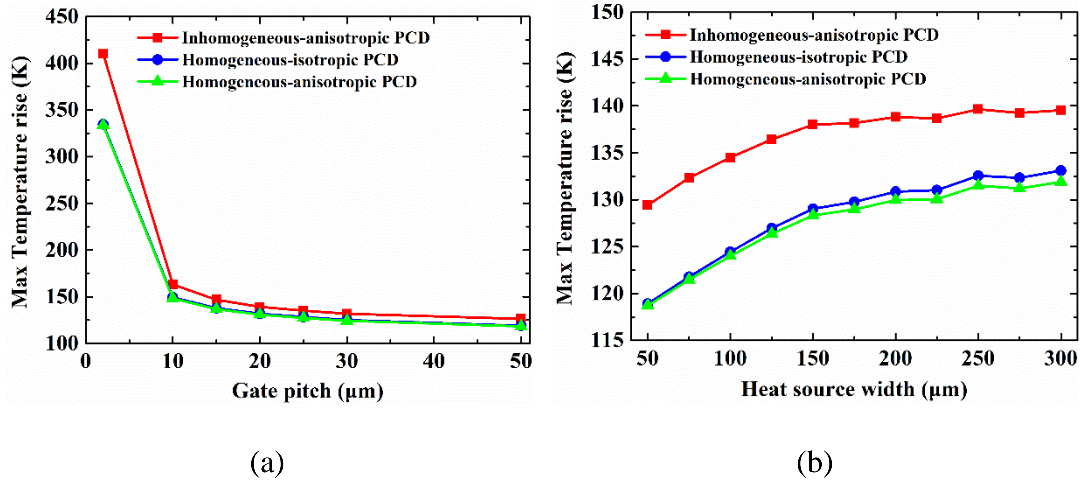

(a) (b)

Figure 5 Dependence of maximum temperature rise on gate pitch (a) and heat source width (b) for TBR of 30 m^2K/GW.

Then we change the base temperature, temperature at the bottom of substrate, and extract the corresponding thermal resistance as a function of power dissipation in Figure 6. For temperatures of RT, 100 and 150 ℃, the contribution of inhomogeneous-anisotropic PCD thermal conductivity remains highest and the rest two are almost the same. The enhancement of the base temperature indicates the deficient heat spreading of the GaN HEMT devices and thus results in an increased

thermal resistance. The thermal resistance rises nonlinearly with the increase of power dissipation and can be modelled with $R_{th} = a \times P_d^2 + b \times P_d + c$. The fitted parameters are listed in Table 3.

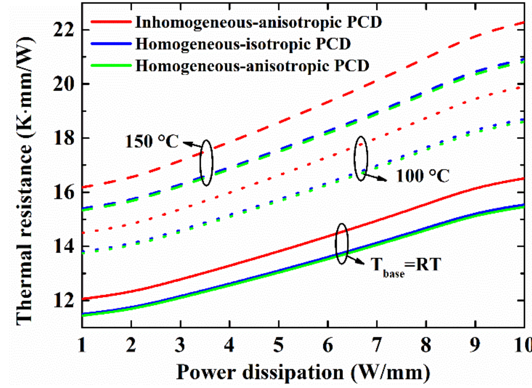

Figure 6 Variation of maximum temperature rise with power dissipation at different base temperature for TBR of 30 m^2K/GW.

Table 3. Fitted parameters from the relation $R_{th} = a \times P_d^2 + b \times P_d + c$.

Base temperature	Thermal conductivity	a (10^{-5})	b (10^{-4})	c (10^{-2})
RT	Inhomogeneous-anisotropic PCD	1.006	4.155	1.150
	Homogeneous-isotropic PCD	0.879	3.807	1.099
	Homogeneous-anisotropic PCD	0.865	3.763	1.092
100 ℃	Inhomogeneous-anisotropic PCD	1.269	4.989	1.384
	Homogeneous-isotropic PCD	1.108	4.565	1.320
	Homogeneous-anisotropic PCD	1.091	4.517	1.311
150 ℃	Inhomogeneous-anisotropic PCD	1.463	5.587	1.544
	Homogeneous-isotropic PCD	1.277	5.111	1.472
	Homogeneous-anisotropic PCD	1.258	5.059	1.462

Finally, the effects of different substrates (inhomogeneous-anisotropic PCD, SiC, Si and GaN) on maximum channel temperature are illustrated considering each experimentally optimized TBR values from Refs. [5,23,24,26], as summarized in Table 2. Except for the thermal conductivity of GaN homoepitaxy on GaN substrate, whose value is reported as high as 260 W/(m·K)[27].The anisotropic SiC thermal conductivity is also introduced with $\eta_{SiC}=\kappa_{SiC,\ in\text{-}plane}/\kappa_{SiC,\ cross\text{-}plane}=0.65$[13].

As shown in Figure 7, the maximum temperature occurs at the proximity of active region in the transistor and is the largest in Si, then GaN, anisotropic SiC, isotropic SiC and PCD, which basically follows the orders of each thermal conductivities. Figure 8 (a) displays the power dissipation dependent temperature rises of inhomogeneous-anisotropic PCD with different TBR of 6.5, 30 60 m^2K/GW, anisotropic/isotropic SiC, Si and GaN, among which Si substrate is the worst heat spreading layer, and the temperature rise can be reduced remarkably when using other substrate materials, especially for large power dissipation. The SiC substrate is superior to GaN substrate and the anisotropy in its thermal conductivity has minor effect on device junction temperature. PCD substrate proves its superior heat conducting capability even for large TBR value. The anisotropy ratios of the maximum temperature rise originating from isotropic versus anisotropic thermal conductivity in SiC and inhomogeneous-anisotropic versus homogeneous-isotropic thermal conductivity PCD are illustrated in figure 8 (b). The anisotropy ratio is evidently larger for SiC substrate than that for PCD substrate and becomes enlarged at higher power density due to more concentrated heat in the transistor.

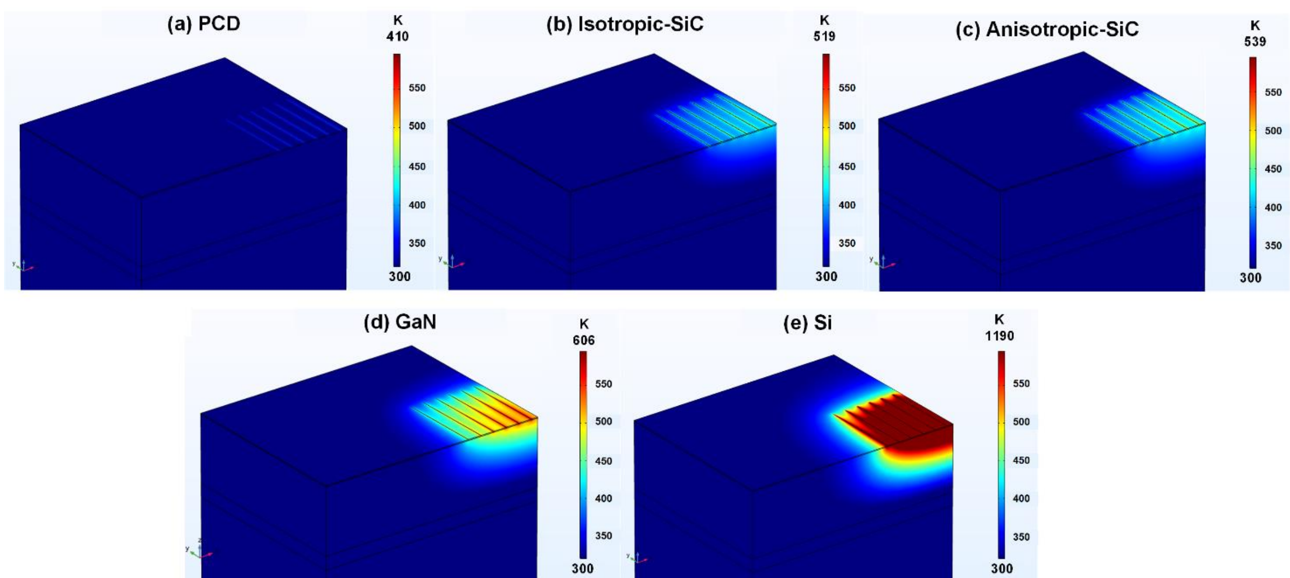

Figure 7 Temperature distribution of the transistor with inhomogeneous-anisotropic PCD, isotropic SiC, anisotropic SiC, GaN and Si substrates at power dissipation of 10 W/mm.

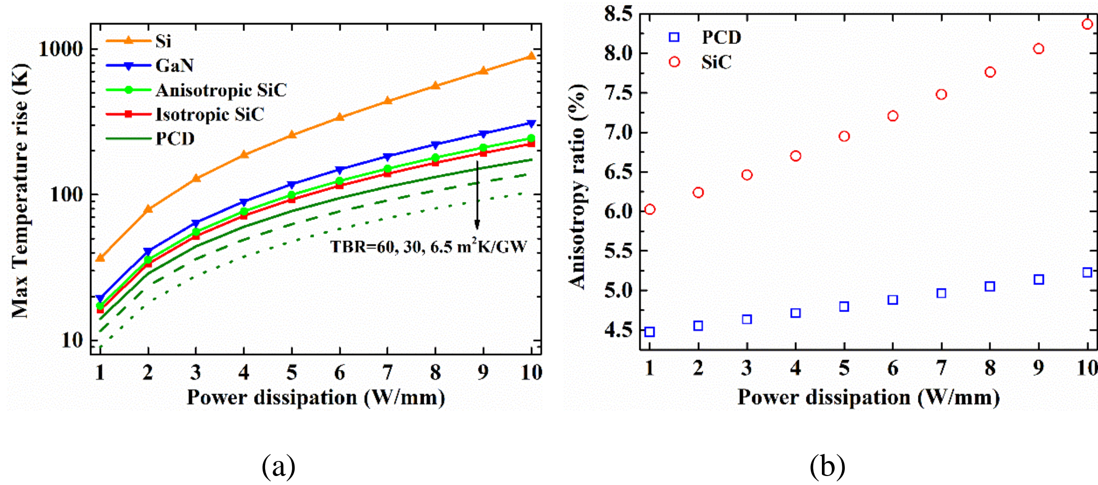

(a) (b)

Figure 8 The effect of power dissipation on maximum temperature rise for different substrate materials (a) and anisotropic ratio of SiC and PCD (b).

4. Conclusion

The FEM heat simulation is used to estimate the effect of inhomogeneous-anisotropic PCD thermal conductivity and anisotropic GaN thermal conductivity on channel temperature. The results show that neglecting solely the anisotropy in GaN thermal conductivity underestimates the channel temperature by 7.3~15.5 K for TBR of 6.5~60 m^2K/GW, while the differences for ignoring the anisotropic/space-variant PCD thermal conductivity are relatively large at small TBR, about 10 K at TBR of 6.5 m^2K/GW and reduce to 6~7 K for TBR of 60 m^2K/GW. For the case with homogeneous/isotropic PCD thermal conductivity and isotropic GaN thermal conductivity, the errors are the largest (over 15 K) at small TBR and display an increasing tendency when TBR increases. Moreover, we analyze the dependences of channel temperature on several parameters, as GaN thickness, gate pitch, heat source width, base temperature, power and substrate material, and find that an optimum GaN layer thickness of ~3 μm exists for 0.5 μm-long gate at TBR=10 m^2K/GW.

Restraining the length of gate pitch is an effective way to reduce the channel temperature, while the impact of narrowing heat source width is limited. The thermal resistance increases with increasing base temperature and power dissipation. Limited by in-plane thermal conductivity, PCD is still the most effective heat spreading layer among GaN, SiC and Si substrates.

Acknowledgments

This work was supported by the open project of Key Laboratory of Wide Band-gap Semiconductor Materials, Ministry of Education (Grant Nos. Kdxkf2019-01).

References

[1] Sood A., Cho J., Hobart K. D., Feygelson T. I., Pate B. B., Asheghi M., Cahill D. G., Goodson K. E.: Anisotropic and inhomogeneous thermal conduction in suspended thin-film polycrystalline diamond. J. Appl. Phys. **119**(17), 175103 (2016)

[2] Cho J., Francis D., Altman D. H., Asheghi M., Goodson K. E.: Phonon conduction in GaN-diamond composite substrates. J. Appl. Phys. **121**(5), 055105 (2017)

[3] Anaya H. S. J., Pomeroy J., Kuball M.: Thermal management of GaN-on-diamond high electron mobility transistors: Effect of the nanostructure in the diamond near nucleation region. 15th IEEE Intersoc. Conf. Therm. Thermomech. Phenom. Electron. Syst. (ITherm), Las Vegas, NV, USA, (2016)

[4] Zou B., Sun H., Guo H., Dai B., Zhu J.: Thermal characteristics of GaN-on-diamond HEMTs: Impact of anisotropic and inhomogeneous thermal conductivity of polycrystalline diamond. Diamond Relat. Mater. **95**, 28 (2019)

[5] Song C., Kim J., Lee H., Cho J.: Fundamental limits for near-junction conduction cooling of high power GaN-on-diamond devices. Solid State Commun. **295**, 12-15 (2019)

[6] Guo H., Kong Y., Chen T.: Thermal simulation of high power GaN-on-diamond substrates for HEMT applications. Diamond Relat. Mater. **73**, 260-266 (2017)

[7] Hodges C., Calvo J. A., Stoffels S., Marcon D., Kuball M.: AlGaN/GaN field effect transistors for power electronics—Effect of finite GaN layer thickness on thermal characteristics. Appl. Phys. Lett. **103**(20), 202108 (2013)

[8] Zhang H., Chen X., Jho Y. D., Minnich A. J.: Temperature-Dependent Mean Free Path Spectra of Thermal Phonons Along the c-Axis of Graphite. Nano Lett. **16**, 1643-1649 (2016)

[9] Sood A., Xiong F., Chen S., Cheaito R., Lian F., Asheghi M., Cui Y., Donadio D., Goodson K. E., and Pop E.: Quasi-Ballistic Thermal Transport Across MoS2 Thin Films. Nano Lett. **19**, 2434-2442 (2019)

[10] Koh Y. K., Cao Y., Cahill D. G., Jena D.: Heat-Transport Mechanisms in Superlattices. Adv. Funct. Mater. **19**, 610-615 (2009)

[11] Bougher T. L., Yates L., Lo C. F., Johnson W., Graham S., Cola B. A.: Thermal Boundary Resistance in GaN Films Measured by Time Domain Thermoreflectance with Robust Monte Carlo Uncertainty Estimation. Nanoscale Microscale Thermophys. Eng. **20**(1), 22-32 (2016)

[12] Ziade E., Jia Y., Brummer G., Nothern D., Moustakas T., Schmidt A. J.: Thermal transport through GaN–SiC interfaces from 300 to 600 K. Appl. Phys. Lett. **107**(9), 091605 (2015)

[13] Cho J., Bozorg-Grayeli E., Altman D. H., Asheghi M., Goodson K. E.: Low Thermal Resistances at GaN–SiC Interfaces for HEMT Technology. IEEE Electron Device Lett. **33**(3), 378-380 (2012)

[14] Cho J., Li Y., Hoke W. E., Altman D. H., Asheghi M., Goodson K. E.: Phonon scattering in strained transition layers for GaN heteroepitaxy. Phys. Rev. B **89**(11), 115301 (2014)

[15] Wang Z., Alaniz J. E., Jang W., Garay J. E., Dames C.: Thermal Conductivity of Nanocrystalline Silicon: Importance of Grain Size and Frequency-Dependent Mean Free Paths. Nano Lett. **11**, 2206-2213 (2011).

[16] Li W., Mingo N., Lindsay L., Broido D. A., Stewart D. A., Katcho N. A.: Thermal conductivity of diamond nanowires from first principles. Phys. Rev. B **85**(19), 195436 (2012)

[17] Yates L., Anderson J., Gu X., Lee C., Bai T., Mecklenburg M., Aoki T., Goorsky M. S., Kubal l M., Piner E. L., Graham S.: Low Thermal Boundary Resistance Interfaces for GaN-on-Diamond Devices. ACS Appl. Mater. Interfaces **10**(28), 24302-24309 (2018)

[18] Dong H., Wen B., Melnik R.: Relative importance of grain boundaries and size effects in thermal conductivity of nanocrystalline materials. Sci. Rep. **4**, 7037 (2014)

[19] Zhai W., Zhang J., Chen X., Bu R., Wang H., Hou X.: FEM thermal and stress analysis of bonded GaN-on-diamond substrate. AIP Adv. **7**(9), 095105 (2017)

[20] Chen X., Zhai W., Zhang J., Bu R., Wang H., Hou X.: FEM thermal analysis of high power GaN-on-diamond HEMTs. J. Semicond. **39**(10), 104005 (2018)

[21] Park K., Bayram C.: Thermal resistance optimization of GaN/substrate stacks considering thermal boundary resistance and temperature-dependent thermal conductivity. Appl. Phys. Lett. **109**(15), 151904 (2016)

[22] Wang A., Tadjer M. J., Calle F.: Simulation of thermal management in AlGaN/GaN HEMTs with integrated diamond heat spreaders. Semicond. Sci. Technol. **28**, 055010 (2013)

[23] Zhou Y., Anaya J., Pomeroy J., Sun H., Gu X., Xie A., Beam E., Becker M., Grotjohn T. A., Lee C., and Kuball M.: Barrier Layer Optimization for Enhanced GaN-on-diamond Device Cooling. ACS Appl. Mater. Interfaces **9**(39), 34416-34422 (2017)

[24] Yates L., Bougher, T. L. Beechem T., Cola B. A., Graham S.: The Impact of Interfacial Layers on the Thermal Boundary Resistance and Residual Stress in GaN on Si Epitaxial Layers. ASME 2015 International Technical Conference and Exhibition on Packaging and Integration of Electronic and Photonic Microsystems collocated with the ASME 2015 13th International Conference on Nanochannels, Microchannels, and Minichannels San Francisco, California, USA, July 2015.

[25] Babic D. I.: Optimal AlGaN/GaN HEMT Buffer Layer Thickness in the Presence of an Embedded Thermal Boundary. IEEE Trans. Electron Devices, **61**(4), 1047-1053 (2014)

[26] Sommet R., Mouginot, G. Quéré R., Ouarch Z., Camiade M.: Thermal modeling and measurements of AlGaN/GaN HEMTs including Thermal Boundary Resistance. Microelectron. J. **43**, 611-617 (2012)

[27] Killat N., Montes M., Pomeroy J. W., Paskova T., Evans K. R., Leach J., Li X., Özgür Ü.,. Morkoç H, Chabak K. D., Crespo A., Gillespie J. K., Fitch R., Kossler M., Walker D. E., Trejo M., Via G. D., Blevins J. D., Kuball M.: Thermal Properties of AlGaN/GaN HFETs on Bulk GaN Substrates. IEEE Electron Device Lett. **33**(3), 366-368 (2012)